



HAL
open science

Numerical investigations of the tunnel environment effect on the performance of energy tunnels

Chunjing Ma, Alice Di Donna, Daniel Dias, Jiamin Zhang

► **To cite this version:**

Chunjing Ma, Alice Di Donna, Daniel Dias, Jiamin Zhang. Numerical investigations of the tunnel environment effect on the performance of energy tunnels. *Renewable Energy*, 2021, 172, pp.1279-1292. 10.1016/j.renene.2021.03.104 . hal-04829489

HAL Id: hal-04829489

<https://hal.science/hal-04829489v1>

Submitted on 19 Dec 2024

HAL is a multi-disciplinary open access archive for the deposit and dissemination of scientific research documents, whether they are published or not. The documents may come from teaching and research institutions in France or abroad, or from public or private research centers.

L'archive ouverte pluridisciplinaire **HAL**, est destinée au dépôt et à la diffusion de documents scientifiques de niveau recherche, publiés ou non, émanant des établissements d'enseignement et de recherche français ou étrangers, des laboratoires publics ou privés.



Distributed under a Creative Commons Attribution - NonCommercial 4.0 International License

Numerical investigations of the tunnel environment effect on the performance of energy tunnels

Chunjing MA¹, Alice DI DONNA¹, Daniel DIAS^{1,2,3*}, Jiamin ZHANG¹

¹ Univ. Grenoble Alpes, CNRS, Grenoble INP**, 3SR, F-38000 Grenoble, France

² Antea Group, Antony, France

³ School of Automotive and Transportation Engineering, Hefei Univ. of Technology, Hefei 230009, China

*Corresponding author, E-mail: daniel.dias@anteagroup.com, Address: 2-6 Place du Général de Gaulle, 92160 Antony, France

**Institute of Engineering Univ. Grenoble Alpes

Abstract: Energy tunnels having lining equipped with heat exchangers as heat or sink resources have gained increasing popularity in recent decades to satisfy the energy demand. This study focuses on numerical simulations based on the continuous operation of thermally activated segmental linings. It aims to analyze the tunnel environment effect on the energy performance of a typical metro tunnel section and estimate the concrete lining role in the heat transfer. Two approaches are expressed to access the system energy efficiency and validated against existing literature data. The numerical results show the influence of the temperature difference between the tunnel air and the circulating fluid and the heat transfer coefficient on the system energy efficiency, which indicates that energy is mainly exchanged with the tunnel environment in winter, but in summer, the surrounding ground plays a major role for the studied case. When evaluating the geothermal potential of an energy tunnel, it is necessary to undertake an initial assessment not only on the ground conditions, but also on the tunnel environment and the concrete lining thermal properties.

Keywords: Energy tunnel, heat power, tunnel environment, numerical modelling, concrete lining

31 *List of symbols*

32	A	Central area of a zone, m^2
33	A_l	Tunnel surface area in contact with the ground, m^2
34	C_{eff}	Effective volumetric specific heat capacity, $J/m^3/K$
35	c_f	Specific heat of circulating fluid, $J/kg/K$
36	c_p	Specific heat capacity at constant pressure, $J/kg/K$
37	c_s	Specific heat of dry solid matrix, $J/kg/K$
38	c_w	Groundwater specific heat, $J/kg/K$
39	D_{in}	Inner diameter of the pipe wall, m
40	D_{out}	Outer diameter of the pipe wall, m
41	f_D	Darcy friction factor
42	h_{eq}	Equivalent convective heat transfer coefficient, $W/m^2/K$
43	h_f	Convective heat transfer coefficient of circulating fluid, $W/m^2/K$
44	h_t	Convective heat transfer coefficient at air-lining interface, $W/m^2/K$
45	k	Hydraulic conductivity, m/s
46	\dot{m}	Mass flow rate, kg/s
47	n	porosity
48	Pr	Prandtl number
49	\dot{Q}	Instantaneous heat power, W or J/s
50	\dot{Q}_l	Instantaneous heat power per unit tunnel lining area, W/m^2
51	Q_{ave}	The average heat power over an operating period, W/m^2
52	q^T	Heat flux, W/m^2
53	q_{cond}^T	Conductive heat flux, W/m^2
54	q_{conv}^T	Convective heat flux, W/m^2
55	q_v^T	Volumetric heat source or sink intensity, W/m^3
56	q_w	Groundwater flow rate, m/s
57	Re	Reynolds number
58	S	Body surface, m^2
59	S_r	Degree of saturation
60	T	Temperature, $^{\circ}C$
61	T_a	Tunnel air temperature, $^{\circ}C$
62	T_f	Temperature of the circulating fluid, $^{\circ}C$
63	T_{in}	Inlet temperature of absorber pipes, $^{\circ}C$
64	T_{ini}	Initial temperature of the domain, $^{\circ}C$
65	T_l	Tunnel lining temperature, $^{\circ}C$
66	T_{out}	Outlet temperature of absorber pipes, $^{\circ}C$
67	T_0	Initial monitored temperature of tunnel air, $^{\circ}C$
68	T_{∞}	Temperature of far field, $^{\circ}C$
69	t	Time, s
70	t_o	Operating time, day
71	V	Zone volume, m^3

72

73 *List of greek letters*

74	λ	Thermal conductivity, W/m/K
75	λ_{eff}	Effective thermal conductivity, W/m/K
76	λ_f	Thermal conductivity of the circulating fluid, W/m/K
77	λ_l	Thermal conductivity of tunnel lining, W/m/K
78	λ_p	Thermal conductivity of the pipe wall, W/m/K
79	λ_s	Solid thermal conductivity, W/m/K
80	λ_w	Groundwater thermal conductivity, W/m/K
81	ρ	Total density, kg/m ³
82	ρ_d	Dry density of the soil, kg/m ³
83	ρ_w	Groundwater density, kg/m ³
84	Ω	Body volume, m ³

85

86 *List of subscripts*

87	x, y, z	Cartesian coordinates, m
88	i, j	zone numbers

89

90 **1. Introduction**

91 It is estimated that 36% of the total final energy consumption in 2017 was used by built
92 environments which represented 39% of the global energy-related CO₂ emissions in 2017 [1].
93 The environmental deterioration is related to the growing energy demand that can be satisfied
94 by increasing energy supply, for example by finding new ways to exploit oil and gas
95 reservoirs. However, sustainable solutions rely on both decreasing the consumption of fossil
96 fuel and developing technologies that harvest renewable energy sources [2].

97 In recent decades, the ground-coupled heat pump (GCHP) system offered one of the best
98 ways of providing sustainable renewable energy in an urban environment where the ground
99 immediately below a city can be utilized as a low-grade energy storage reservoir for its high
100 energy efficiency and environmentally friendly mechanism for cooling and heating demand
101 [3]. A modern application of this technology is represented by the so-called energy
102 geostructures [4–6]. They couple the structural role of geotechnical structures to the low
103 enthalpy geothermal principles, by integrating in the concrete elements a circuit of
104 high-density polyethylene plastic pipes for ground heat exchange. These thermally active
105 systems are mainly related to base slabs, piles and, diaphragm walls [7]. During recent years,
106 increasing considerations were paid on how this heat transfer technology could be extended
107 to tunnels as a renewable energy source for energy networks on a city scale [8–10]. The
108 outstanding advantage of energy tunnels is that substantially larger ground volumes and
109 surfaces can be activated for heat exploitation in comparison with other geothermal structures
110 due to their extensive linear characteristics. Urban tunnels are normally built as part of a city
111 and included in the infrastructure planning, which is considered suitable to supply energy to
112 built-up areas [11–13].

113 An increasing number of tunnels are now being excavated by means of full-face TBMs
114 for reducing the construction risk when excavated in weak strata, especially for water-bearing
115 ones. In these cases, the absorber pipes can be simply tied to the reinforcement cage during
116 the concrete segments prefabrication [12]. An early typical energy segmental lining called
117 ‘Energietübbing’ was designed by Ed. Züblin AG and Rehau AG & Co [15] with the pipeline

118 running parallel to the tunnel axis, (Fig. 1a). More recently, a novel energy tunnel precast
119 segmental lining containing two pipes layers called ‘ENERTUN’ characterized by the main
120 direction of absorber pipes perpendicular to the tunnel axis and a double circuit to facilitate
121 the heat exchange with both ground and air was proposed by Barla & Di Donna [16] (Fig. 1b)
122 and patented by the Politecnico di Torino (Italy).

123

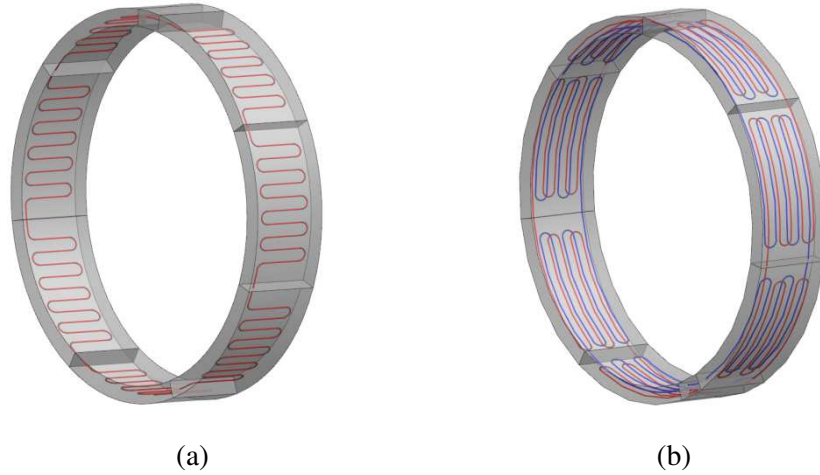


Fig. 1. Existing energy segmental linings: (a) ‘Energietübbingand’ (b) ‘ENERTUN’.

127 Having the ground on one side and the air on the other side is a typical condition of
128 tunnels and diaphragm walls, differently from energy piles for instance. Thus the thermal
129 efficiency of an energy tunnel is influenced by both the tunnel air and the surrounding ground
130 conditions [17]. The investigation of the thermal exchange with the tunnel air is essential: the
131 tunnel environment may vary due to inside activities and results in heat exchange alterations
132 between the tunnel air and concrete lining. The concrete lining acts as a heat transfer medium
133 that wraps the heat absorber pipes, its role also deserves to be studied. Zhang et al. [18]
134 carried out a laboratory model test to evaluate the coupling effects of the ventilation and
135 groundwater flow on the thermal performance of energy tunnel linings. The results revealed
136 that the tunnel ventilation effectively enhances the heat exchange between the absorber pipes
137 and the surrounding rock.

138 Some studies investigated the effects of tunnel air on the energy performance through
139 numerical modelling [19]. Thermo-hydro numerical analyses conducted by Tinti et al. [20]

140 indicated that the tunnel air and the groundwater flow need to be modelled considering both
141 conduction and convection mechanisms in order to capture its accurate thermal status.
142 Bourne-Webb et al. [21] showed that energy is mainly exchanged with tunnel environment
143 rather than with ground and constant temperature boundary can be non-conservative.
144 Therefore, convective boundary conditions may allow a closer representation of the true state
145 of an energy tunnel, and the convective heat transfer coefficient is a main parameter that
146 relates of the tunnel environment to heat transfer rates. Peltier et al. [22] investigated the
147 relationships between the convective heat transfer coefficient and average airflow velocity for
148 different concrete surface roughnesses, which provides a way to estimate the convective heat
149 transfer coefficient value for a tunnel. To assess the influence of some parameters including
150 the convective heat transfer coefficient on the geothermal potential of energy tunnels,
151 sensitivity analyses were also carried out by Insana et al. [23], and the effect of this
152 coefficient variation on the amount of heat flowing between tunnel environment and the
153 lining was observed.

154 Despite the previous works, not a lot of data relating to the relationship between tunnel
155 environment and heat transfer rate of energy tunnels has been published and no quantitative
156 details between the environmental conditions and the ground conditions are provided, which
157 motivates the present study. The work presented here is based on numerical analyses. and its
158 contributions are mainly the following ones: (i) two numerical approaches for quantifying the
159 thermal efficiency of an energy tunnel are proposed and critically compared as possible
160 methods to study the influence of tunnel environment, (ii) design charts are provided, for both
161 heating and cooling modes, to predict the average thermal efficiency as a function of the
162 tunnel environment conditions, and (iii) the contributions of different components in an
163 energy tunnel system and the thermal property effect of concrete lining are investigated.

164 **2. Numerical modelling**

165 The heat transfer of a ground heat exchanger system (GHEs) is a complicated process
166 owing to the conjugate heat transfer of various mechanisms. Generally, heat transfer in soils

167 is induced by three main mechanisms: conduction, convection, and water phase change, also
168 known as latent heat of vaporisation. Radiation in soils usually plays a negligible role for heat
169 transfer and it is excluded from formulations [3,24].

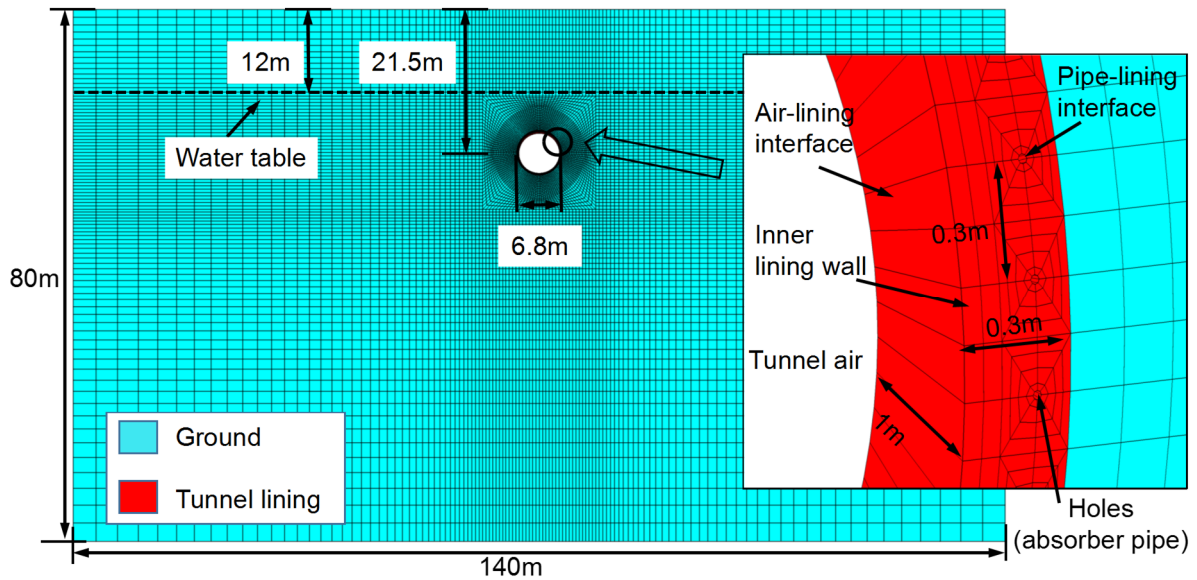
170 Heat transfer by conduction occurs by a collision process between the soil solids
171 molecules, water and pore air. Heat conduction through air is not of great importance but its
172 effect should be included in the soil thermal conductivity calculation [25]. The heat transfer
173 by convection through porous media includes free convection, which accounts for the fluid
174 motion caused by the density differences due to the temperature variations, and the forced
175 convection, in which the heat is carried by the fluid motion (underground seepage). Water
176 phase changes, including water freezing and ice melting, as well as evaporation which leads
177 to vapor diffusion and subsequent condensation, may also produce latent effects on heat
178 transfer, but such effects are negligible in the applications studied here.

179 In the following work, unless specified otherwise, all model components are assumed to
180 have constant thermal and hydraulic properties. The conductive fluid heat transfer along the
181 pipes axis is ignored [26,27], and the thermal contact resistance at the interface between the
182 tunnel lining and the surrounding ground and between the tunnel lining and the absorber pipe
183 is also considered as negligible. In this study, the ground where the excavation takes place, is
184 considered as fully saturated. Thus, the following four mechanisms are involved in the
185 numerical calculations: (1) conductive and convective heat transfer in saturated ground, (2)
186 conductive heat transfer in the segmental lining, (3) convective heat transfer between heat
187 fluid and pipes, and (4) convective heat transfer between tunnel air and segmental lining.

188 *2.1. Numerical model geometry*

189 The tunnel geometry was taken from [28] for the sake of validation and comparison. In
190 order to reduce the complexity and computational time, a 1m-thick model based on the Turin
191 Metro Line 1 section profile was developed using the finite difference software FLAC3D
192 (Itasca 2016). The geometry of this model is presented in Fig. 2. The model is composed of
193 31442 nodes and 15246 hexahedral zones. The modelled tunnel has a 30 cm-thick segmental

194 lining with an outer diameter of 6.8m and so that the inner diameter is equal to 6.2m. The
 195 tunnel buried depth is between 18.1m and 24.9m. The excavation was conducted below the
 196 water table which is at 12m below the ground surface. The whole domain is 80m high, 140m
 197 wide and 1m thick. The width is equal to twenty times the outer tunnel diameter, which
 198 allows the boundary effects to be ignored.



199
 200 **Fig. 2.** The geometry and dimension of finite difference model.

201 The absorber pipes are represented as holes in the model, having a diameter of 25 mm.
 202 The external holes boundaries correspond to the pipe-lining interfaces. The center of each
 203 pipe is at 20 cm from the air-lining interface, with a spacing of 30 cm. No mesh zones are
 204 used for the pipes walls. However, the outside diameter and the pipe walls thickness, which
 205 are respectively equal to 25 mm and 2.3 mm, are taken into account in the computation of the
 206 convective heat transfer coefficient on the pipe-lining interface, as is detailed in section 2.3.

207 *2.2. Mathematical formulation*

208 When only the conductive heat transfer mechanism is considered, the temperature and
 209 the heat flux components are related through the energy-balance equation and transport laws
 210 derived from the heat conduction Fourier's law. The differential equation for an elementary
 211 volume in cartesian coordinates is obtained by substituting the Fourier's law into the
 212 energy-balance equation:

213
$$\frac{\partial}{\partial x}\left(\lambda \frac{\partial T}{\partial x}\right) + \frac{\partial}{\partial y}\left(\lambda \frac{\partial T}{\partial y}\right) + \frac{\partial}{\partial z}\left(\lambda \frac{\partial T}{\partial z}\right) + q_v^T = \rho c_p \frac{\partial T}{\partial t} \quad (1)$$

214 where λ [W/m/K] is the thermal conductivity and q_v^T [W/m³] is the volumetric heat source or
 215 sink intensity of the medium, ρ [kg/m³] is the mass density of the considered material, and c_p
 216 [J/kg/K] is the specific heat capacity at constant pressure. If the thermal conductivity is
 217 constant, Eq. (1) can be simplified and written as:

218
$$\frac{\partial^2 T}{\partial x^2} + \frac{\partial^2 T}{\partial y^2} + \frac{\partial^2 T}{\partial z^2} + \frac{q_v^T}{\lambda} = \frac{1}{\alpha} \frac{\partial T}{\partial t} \quad (2)$$

219 where $\alpha = \lambda/(\rho c_p)$ is the thermal diffusivity.

220 When also convective-diffusive heat transfer mechanism is considered, the energy
 221 balance becomes:

222
$$C_{eff} \frac{\partial T}{\partial t} + \nabla q^T + \rho_w c_w q_w \nabla T - q_v^T = 0 \quad (3)$$

223 where q^T [W/m²] is the heat flux, q_w [m/s] is the groundwater flow rate, ρ_w [kg/m³] and c_w
 224 [J/kg/K] are respectively the fluid reference density and specific heat. Note that C_{eff} is the
 225 effective specific heat capacity given by:

226
$$C_{eff} = \rho c_p = \rho_d c_s + n S_r \rho_w c_w \quad (4)$$

227 where ρ_d [kg/m³] and c_s [J/kg/K] are respectively the dry density and specific heat, n is the
 228 porosity, and S_r is the degree of saturation.

229 2.3. Thermal and hydraulic initial conditions

230 The temperature of the whole domain, including the water in the aquifer, is initialised to
 231 14 °C, which is assumed to be the undisturbed ground temperature. The position of the
 232 groundwater table is located at a depth of 12.5 m from the surface. The tunnel excavation
 233 takes place below the water table in the homogeneous, fully saturated ground. The material
 234 properties of the tunnel segmental lining and ground are taken from Barla et al. [28] and
 235 listed in Table 1. The same geometry and material properties were also assumed by Ogunleye
 236 et al. [26], and their results are also used here for validation.

237 **Table 1**

238 Material parameters.

Parameters	Ground	Concrete lining	Groundwater	Pipe
Thermal conductivity, λ [W/m/K]	2.8	2.3	0.65	0.38
Volumetric heat capacity, ρc_p [MJ/m ³ /K]	2.0	2.19	4.2	-
Initial temperature, T_{ini} [°C]	14	14	14	-
Horizontal hydraulic conductivity, k_x [m/s]	4.15×10^{-3}	10^{-16}	-	-
Vertical hydraulic conductivity, k_y [m/s]	2.08×10^{-4}	10^{-16}	-	-
Porosity, n [-]	0.25	0.05	-	-

239 *2.4. Thermal and hydraulic boundary conditions*

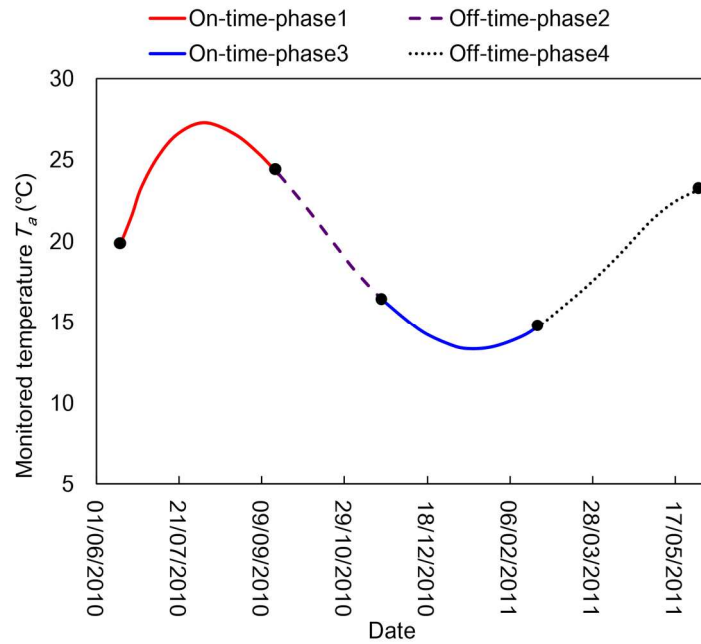
240 Adiabatic boundary conditions are imposed on the vertical surfaces crossing the tunnel
241 axis, meaning that no heat flux occurs across these boundaries. Constant temperature
242 boundary conditions are considered on the far-field boundaries (top and bottom model
243 boundaries as well as on the lateral edges of the model). The temperature is thereby fixed to
244 the initial temperature applied to the whole domain (i.e. $T_\infty = T_{ini} = 14$ °C).

245 At the interface between the tunnel air and the concrete lining, the heat transfer is
246 described by a convective boundary condition related to the airflow profile over the concrete
247 surface [3,7,15,20]. The heat flux component, which is normal to the interface between the
248 tunnel air and the lining, is written as:

$$249 \quad q^T = h_t (T_l - T_a) \quad (5)$$

250 where h_t [W/m²/K] is the convective heat transfer coefficient that is related to the airflow
251 velocity and tunnel lining surface roughness [22], T_l [K] is the tunnel lining temperature near
252 the interface, and T_a is the tunnel air temperature. The tunnel environment is complex and
253 depends on many factors, difficult to be quantified, which includes the trains circulation,
254 ventilation and, external climate conditions. For the sensitivity analysis performed in this
255 study, h_t is considered to vary between 2.5 and 25 W/m²/K [21,29]. The boundaries becomes
256 adiabatic when $h_t = 0$ W/m²/K.

257 According to Eq. (5), the tunnel temperature value T_a also plays a significant role in the
 258 heat transfer performance. Fig. 3 shows the polynomial regression of the measured tunnel air
 259 temperature recorded in the Turin Metro from June 2010 to May 2011 [26,28]. The
 260 measurement data taken from this underground tunnel reveals a seasonal oscillation. In the
 261 present study, this curve was subdivided into four phases (Fig. 3). The first 90-days phase
 262 (June to August) was selected for the simulations of the heat injection period in summer,
 263 while a 90-days period (December to February) over the third phase was used for the
 264 simulations of the heat extraction period during winter. This phase represents the highest
 265 heating demand period. The system is considered to be off in phase 2 (September to
 266 November) and phase 4 (March to May) in which the consumption of energy is the lowest.



267
 268 **Fig. 3.** Polynomial regression of the tunnel internal temperature monitored at the metro Torino Metro
 269 [28].

270 In terms of hydraulic boundary conditions, pore pressure was fixed on both sides of the
 271 model, according to an hydrostatic distribution. The bottom and vertical surfaces crossing the
 272 tunnel axis are considered to be impermeable boundaries. The thermal and hydraulic
 273 boundary conditions are summarized in Table 2, together with the thermal load which is
 274 imposed in the pipes as a boundary conditions, as detailed in the next section.

275 **Table 2**

276 Boundary conditions.

	Boundary	Type	Value
Thermal	Lateral sides	Temperature fixed	$T_{mi} = 14$ [°C]
	Top and bottom surfaces	Temperature fixed	$T_{mi} = 14$ [°C]
	Vertical surfaces	Adiabatic	-
	Air-lining interface	Convective	$h_t = 0 - 25$ [W/m ² /K] $T_a =$ see Fig. 7
	Circulating fluid	Convective	$T_{in} = 4.4$ and 27.4 [°C] $h_{eq} = 139$ [W/m ² /K]
Hydraulic	Lateral sides	Pressure imposed	- [Pa]
	Vertical and bottom surfaces	Impermeable	- [Pa]

277 *2.5. Thermal load on the absorber pipes*

278 The thermal load on absorber pipes can be considered as a simplified convective
279 boundary condition that is imposed on the pipe-lining interface.

280 The radial heat flux applied through the boundary domain surrounding the holes in the
281 direction of a unit vector n can be expressed as :

$$282 \quad q^T = -\lambda_l \frac{\partial T}{\partial n} = \begin{cases} h_{eq}(T_l - T_f) & \text{during phase 1 and phase 3} \\ 0 & \text{during phase 2 and phase 4} \end{cases} \quad (6)$$

283 where λ_l is the tunnel lining thermal conductivity, T_l is the tunnel lining temperature around
284 the holes, T_f is the temperature of the circulating fluid, and h_{eq} [W/m²/K] is the equivalent
285 convective heat transfer coefficient. For simplicity, the value of h_{eq} can be defined as Eq. (7)
286 by combining the thermal conductivity of the pipe wall λ_p [W/m/K] and the convective heat
287 transfer coefficient of circulating fluid h_f [W/m²/K] [3].

$$288 \quad h_{eq} = \left[\frac{D_{out}}{2\lambda_p} \ln\left(\frac{D_{out}}{D_{in}}\right) + \frac{D_{out}}{D_{in}h_f} \right] \quad (7)$$

289 where D_{out} [m] is the outer diameter of the pipe wall and D_{in} is the inner one. The value of h_f

290 can be obtained from the Dittus-Boelter equation [30] for a turbulent flow:

$$291 \quad h_f = 0.023 Re^{0.8} Pr^n \frac{\lambda_f}{D_{in}} \quad (8)$$

292 where Re is the Reynolds number, Pr is the Prandtl number, λ_f [W/m/k] is the thermal
293 conductivity of the circulating fluid, $n=0.4$ for heating and 0.3 for cooling of the fluid. This
294 equation is valid for $Re \geq 1 \times 10^5$, $0.6 \leq Pr \leq 160$, $L/D \geq 10$, L is the length of the pipe, and D
295 is the diameter of the pipe.

296 For $Re < 1 \times 10^5$, the Dittus-Boelter equation is no longer recommended because the
297 deviations increase significantly [31]. Thus, the calculation of h_f can be derived from the
298 Gnielinski correlation [32] for turbulent flow in smooth tubes as follows:

$$299 \quad h_f = \frac{(f_D/8)(Re-1000)Pr}{1+12.7(f_D/8)^{1/2}(Pr^{2/3}-1)} \cdot \frac{\lambda_f}{D_{in}} \quad (9)$$

300 where f_D is the Darcy friction factor for smooth tubes that can be obtained from the first
301 Petukhov equation [33]:

$$302 \quad f_D = (0.79 \ln(Re) - 1.64)^{-2} \quad (10)$$

303 The Gnielinski correlation is valid for $3000 \leq Re \leq 5 \times 10^6$, $0.5 \leq Pr \leq 2000$, $L/D \geq 10$.

304 For simplicity, in this study, the circulating fluid temperature T_f is represented by an
305 average temperature along the pipe length at the steady state [34–36]. T_f is considered to be
306 equal to 4.4 °C for the heating mode and 27.5 °C for the cooling mode according to [37]
307 when the groundwater flow rate is equal to 0 m/d.

308 **3. Assessment of exchanged heat**

309 *3.1. Numerical approaches*

310 Various numerical approaches were used in literature to investigate the thermal
311 efficiency of energy geostructures. When the pipes are directly modelled, the exchanged heat
312 can be computed as [3,23,26,28,37]:

$$313 \quad \dot{Q} = \dot{m} c_f (T_{out} - T_{in}) \quad (11)$$

314 where \dot{Q} [W or J/s] is the heat power, \dot{m} [kg/s] and c_f [J/kg/K] are the mass flow rate and the
 315 specific heat of circulating fluid, and T_{out} and T_{in} are the outlet and inlet temperatures of the
 316 pipes respectively. The instantaneous heat power exchanged by the tunnel lining per unit
 317 surface area \dot{Q}_l [W/m²] can be computed as:

$$318 \quad \dot{Q}_l = \frac{\dot{Q}}{A_l} \quad (12)$$

319 where A_l [m²] is the tunnel surface area in contact with the ground.

320 In other studies, the pipes network are not directly modeled and a thermal loading was
 321 applied instead [38,39]. In the present work, this second approach was chosen and
 322 consequently Eq. (11) is not employed, because this model represents only a section of the
 323 energy tunnel. Thus, defining an appropriate method for the calculating heat exchanged for
 324 this model is needed. In this study, two approaches were developed for estimating the
 325 instantaneous heat exchange of the energy tunnel lining per unit surface area (see approach 1
 326 and 2 below). The average heat power over an operating period Q_{ave} [W/m²] can then be
 327 calculated by dividing the total energy exchanged by the operating time t_o [day]:

$$328 \quad Q_{ave} = \int_0^t \dot{Q}_l(t) dt / t_o = \int_0^t \dot{Q}(t) dt / (A_l \cdot t_o) \quad (13)$$

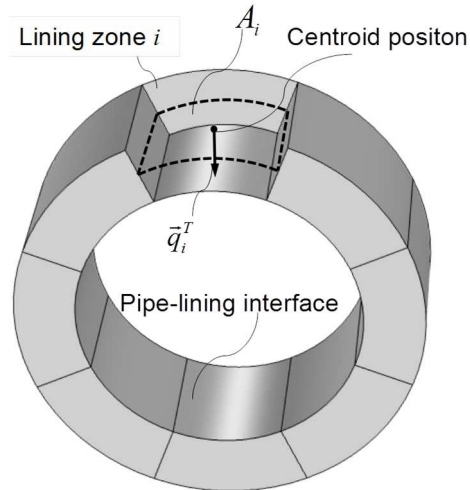
329 Taking into account the heat power at the operation beginning where an unsteady state
 330 exists will overestimate the average thermal efficiency. On the other hand, considering the
 331 steady state value would underestimate it. The heat power for each operation mode was then
 332 averaged after a relative steady state which was defined during a period for which the heat
 333 power variation is lower than 2%.

334 **Approach 1:** In this approach, hollow cylinders wrapping the holes (absorber pipes) are
 335 generated with a radial mesh. Thanks to these closed rings, all the heat exchanged with the
 336 pipes flows through the zones in the layers close to the hole. The instantaneous total heat
 337 power exchanged between the pipes and system can be thereby obtained by summing the
 338 energy flow per unit time through each lining zone around the holes. Assuming a total of m
 339 eligible zones wrapping the holes, the equation can be expressed as follows:

340
$$\dot{Q} = \sum_{i=1}^m \dot{Q}_i = \sum_{i=1}^m |\vec{q}_i^T| A_i \quad (14)$$

341 For the i^{th} zone, the heat power \dot{Q}_i can be obtained by the product of the heat flux vector
 342 module \vec{q}_i^T [W/m²] and the central area A_i [m²] (Fig. 4). The direction of \vec{q}_i^T is normal to
 343 the pipe-tunnel lining interface.

344 This approach requires less data and has a high computational efficiency. However, it
 345 imposes to adapt the mesh and cannot reflect properly the heat transfer mechanism variation
 346 in each component of the thermally activated system (lining, ground and air-lining interface),
 347 nor evaluate the contribution of the conductive and convective heat exchanged under
 348 different ground conditions.



349
 350 **Fig. 4.** Heat transfer through the zone i around a pipe section.

351 **Approach 2:** This approach is an extension of the one developed by Rammal and
 352 co-workers [38] and Delerablee and co-workers [39] for energy walls. The Gauss's theorem,
 353 also called the divergence theorem, allows to link the heat power to its divergence using the
 354 following equation:

355
$$\iint_{\partial\Omega} \vec{q}^T d\vec{S} = \iiint_{\Omega} \text{div}(\vec{q}^T) d\Omega \quad (15)$$

356 where Ω is the body volume that is subjected to \vec{q}^T , and S is the body surface. The
 357 calculation of the divergence allows the inlet and outlet fluxes from a ground volume to be
 358 calculated.

359 Thus, for the convective-diffusive heat transfer condition, Eq. (3) in its differential form
 360 can be expressed as:

$$361 \quad \rho c_p \frac{\partial T}{\partial t} + \text{div}(\vec{q}_{cond}^T) + \text{div}(\vec{q}_{conv}^T) - q_v^T = 0 \quad (16)$$

362 where \vec{q}_{cond}^T [W/m²] is the conductive heat flux, while \vec{q}_{conv}^T [W/m²] is the convective heat
 363 flux vector. The internal volumetric heat intensity $q_{v,j}^T$ of a ground zone is equal to zero as
 364 there is no heat source in it, but for each zone in contact with the tunnel air, as it acts as a heat
 365 resource or a heat sink in this system, its value can be defined as:

$$366 \quad q_{v,j}^T = \frac{|\vec{q}_j^T| A_j}{V_j} \quad (17)$$

367 where V_j [m³] is the volume of the j^{th} zone, and $q_{v,j}^T$ is positive when the heat is transferred
 368 from the tunnel environment to the tunnel lining and negative when heat flow is in the
 369 opposite direction. The divergence of the convective heat flux can be computed as:

$$370 \quad \text{div}(\vec{q}_{conv}^T) = \rho_w c_w (\vec{q}_w \cdot \vec{\nabla} T + \text{div}(\vec{q}_w) \cdot T) \quad (18)$$

371 As the water is considered incompressible, the divergence of the Darcy velocity is equal
 372 to zero, and then the equation becomes:

$$373 \quad \text{div}(\vec{q}_{conv}^T) = \rho_w c_w \vec{q}_w \cdot \vec{\nabla} T \quad (19)$$

374 According to the Fourier's law:

$$375 \quad \vec{q}_{cond}^T = -\lambda_{eff} \vec{\nabla} T \quad (20)$$

376 where λ_{eff} [W/m/K] is the effective thermal conductivity, which is isotropic in the convection
 377 formulation. λ_{eff} is defined in terms of the solid and fluid thermal conductivities, λ_s [W/m/K]
 378 and λ_w [W/m/K], by the equation:

$$379 \quad \lambda_{eff} = \lambda_s + n S_r \lambda_w \quad (21)$$

380 Thus, Eq. (19) can be written:

$$381 \quad \text{div}(\vec{q}_{conv}^T) = -\frac{\rho_w c_w \vec{q}_w \cdot \vec{q}_{cond}^T}{\lambda_{eff}} \quad (22)$$

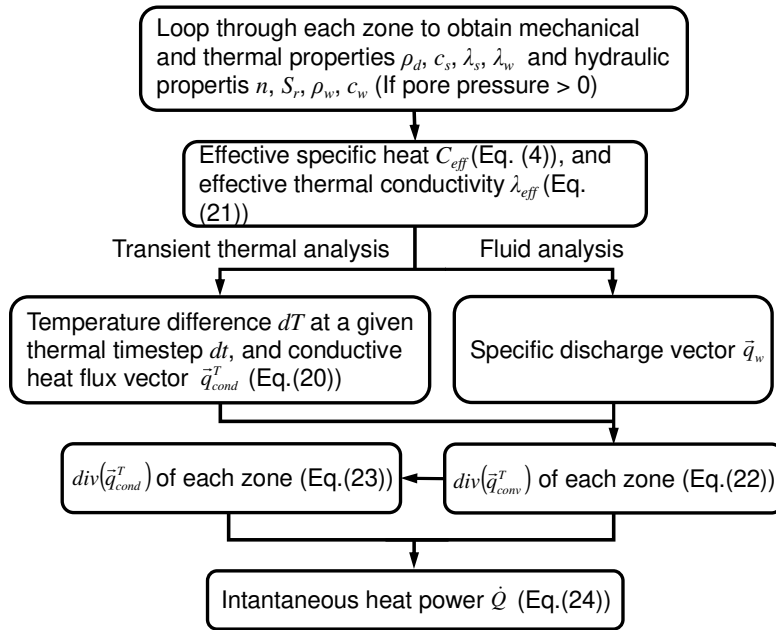
382 Substituting this relation into Eq. (16), it becomes:

$$383 \quad \text{div}(\vec{q}_{cond}^T) = \frac{\rho_w c_w \vec{q}_w \cdot \vec{q}_{cond}^T}{\lambda^T} - \rho c_p \frac{\partial T}{\partial t} + q_v^T \quad (23)$$

384 The instantaneous heat power exchanged can be calculated by the following equation:

$$385 \quad \dot{Q} = \sum_{\Omega} \int [\text{div}(\vec{q}_{cond}^T) + \text{div}(\vec{q}_{conv}^T)] d\Omega = \sum_{\Omega} \int \left(-\rho c_p \frac{\partial T}{\partial t} + q_v^T \right) d\Omega \quad (24)$$

386 The procedure of this approach was implemented in FLAC3D by the flow chart
387 presented in Fig. 5.



388

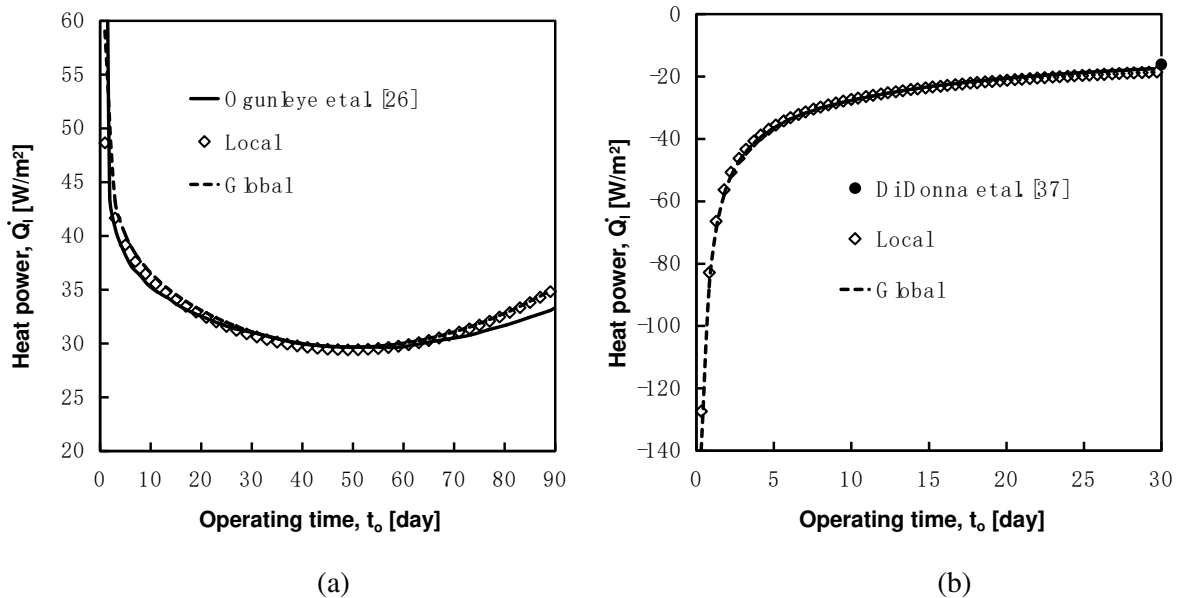
389

Fig. 5. Flow chart showing the program flow of approach 2.

390 When compared with approach 1, approach 2 has a slower calculation speed because it
391 needs to consider the temperature gradient and thermal properties of each zone in the whole
392 domain. Only the heat exchanged by the zones around the absorber pipes is considered in
393 approach 1. Thus, the two approaches in this study are respectively called ‘local’ and ‘global’.
394 In particular, the ‘global’ approach offers the possibility to calculate the amount of heat
395 exchanged by each system component and to distinguish separately the heat transfer by
396 conduction and convection.

397 3.2. Validation of the numerical model and approaches

398 For the validation of the numerical approaches, the model parameters and geometry are
 399 those reported by Barla et al. [28], Ogunleye et al. [26] as well as Di Donna et al. [37]. As
 400 they are all considering the same case study, the initial conditions employed in the literature
 401 are identical to those detailed in section 2.3. Considering the effect of dynamic train loads at
 402 the bottom, only 3/4th of the tunnel lining is considered to be thermally activated for the
 403 comparison with [26]. In this case, the average temperature of the circulating fluid is assumed
 404 to be 5.8 °C. Phase 3 in Fig. 3 was selected as the tunnel air temperature T_a while the heat
 405 transfer coefficient h_t was taken equal to 15 W/m²/K for a 90-day continuous operation for
 406 heating mode. The soil was considered as fully saturated without groundwater flow rate. The
 407 same boundary conditions and properties were adopted for a 30-day cooling operation as in
 408 [37]. For the following sections, the positive value represents extracted heat power, and the
 409 injected heat power is negative. Thus, the magnitude of heat power depends on the absolute
 410 value rather than the sign.



411 (a) 412 (b)
 413 **Fig. 6.** Comparison of heat power per unit of tunnel lining surface: (a) Heating mode, and (b) Cooling
 414 mode.

415 A good agreement can be observed in Fig. 6a against the numerical results presented by
 416 Ogunleye et al. [26] in which the model was validated by referring to the experimental data

417 monitored by Zhang et al. [40]. A higher difference can be observed from 70 to 90 days, and a
418 maximum difference of 5.4% occurs at the operation end. A perfect match between the local
419 and global approaches is shown in Fig. 6a and Fig. 6b (considering a groundwater flow rate
420 of 1.5 m/d). The average heat power obtained from [26] is 31.87 W/m², while the average
421 heat power computed by the local and the global approaches are respectively equal to 32.19
422 W/m² and 32.64 W/m², respectively, which means a difference of 1.0% and 2.4% with
423 respect to the literature data. For the cooling mode (Fig. 6b), different numerical approaches
424 lead to a difference of 0.2% in average injected heat power over 30 days. As the operating
425 time increases (tending towards stability), the heat power difference after a 30-day operation
426 between the literature data and result computed by the local approach is lower than 2.3 W/m².

427 In order to reduce the computing time while maintaining an acceptable accuracy level,
428 the intensity of the mesh near the concrete lining and holes (Fig. 2) was doubled and
429 quadrupled in order to find the optimum mesh size. The average heat power obtained by the
430 global approach from cases in Fig. 6a and 6b for the initial model are 32.64 W/m² and -28.67
431 W/m², respectively, while 32.73 W/m² and -28.52 W/m² were found for the double meshed
432 model and, 32.8 W/m² and -28.43 W/m² for the quadruple meshed model. No significant
433 changes are found for the heating mode (maximum error of 0.5%) and cooling mode
434 (maximum error of 0.8%) in the average heat power beyond the initial mesh size. Therefore,
435 the initial mesh size of proposed model was selected for the following simulations to save
436 computational resources and time. It can be deduced that the energy efficiency can be
437 appropriately calculated by using the proposed model and the two approaches over a period
438 of continuous heat exchange for the heating and cooling modes.

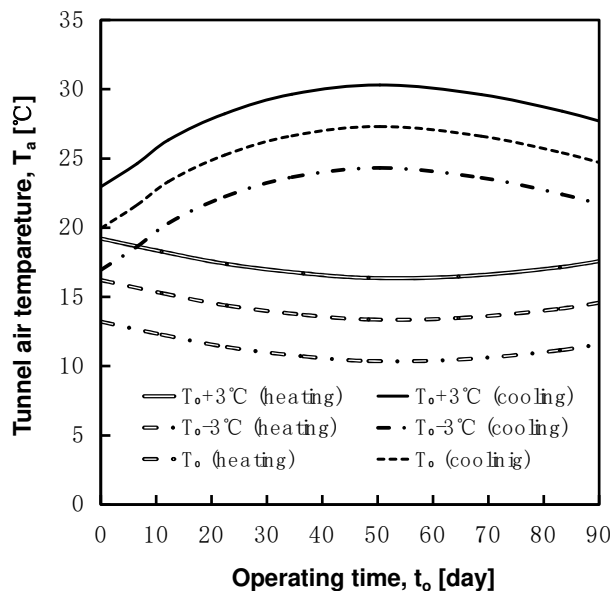
439 **4. Results of numerical analyses on energy performance**

440 To investigate the thermo-hydraulic behaviour and the related energy performance of
441 energy segmental linings, it is of interest to assess the effects of other possibly varying
442 conditions on the thermal efficiency. Two aspects are investigated hereafter: (i) the effect, of
443 varying the air temperature T_a and the heat transfer coefficient h_t on the heat exchange with

444 the tunnel environment; (ii) the contribution of each system's component to the exchanged
 445 heat power. Particular attention is paid to the role of concrete thermal properties on the
 446 contribution of the tunnel lining to the heat exchange. A full ring is thermally activated based
 447 on continuous heating and cooling operations over 90 days for the sake of comparison.

448 *4.1. Tunnel environment influence on total heat power*

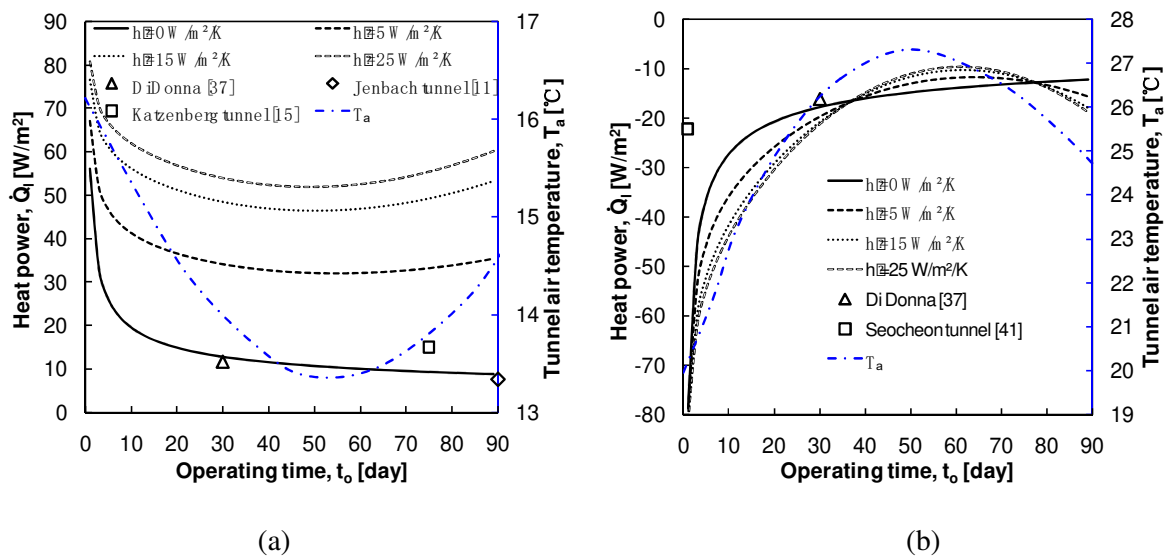
449 According to Eq.(5), the heat transfer coefficient related to the tunnel airflow velocity
 450 and tunnel lining wall roughness, as well as the tunnel air temperature may highly affect the
 451 amount of heat flux between the concrete lining and the tunnel environment. To investigate
 452 the influence of tunnel environment on thermal efficiency, different heat transfer coefficients
 453 and tunnel air temperatures were adopted to characterise various environmental conditions.
 454 The parametric study was performed assuming a saturated soil without groundwater flow rate
 455 by varying the heat transfer coefficient h_t from 0 W/m²/K to 25 W/m²/K and increasing the
 456 tunnel air temperature T_a from T_0-3 °C to T_0+3 °C by increments of 1 °C, where T_0 is the
 457 initial monitored temperature in Fig. 3. The range of T_a during the study period in both modes
 458 is shown in Fig. 7. The other parameters are kept constant as discussed in section 2.



459
 460 **Fig. 7.** The tunnel air temperatures imposed on the air-lining interface

461 The variations of the instantaneous heat power computed by the local approach and for
 462 two operation modes are plotted for all the considered heat transfer coefficients in Fig. 8,

463 together with the air temperature evolution. It can be seen that the instantaneous heat power
 464 has the same varying tendency with the increase or decrease of the tunnel air temperature.
 465 There is an exception for the cases where $h_t = 0 \text{ W/m}^2/\text{K}$. This behaviour shows that the
 466 tunnel air temperature is a sensitive factor for the instantaneous heat power when convection
 467 heat transfer coefficient values vary from 5 to $25 \text{ W/m}^2/\text{K}$. Its sensitivity increases with
 468 increasing the heat transfer coefficient. This implies that the tunnel air temperature is an
 469 important factor to take into account in the design when the heat transfer coefficient is greater
 470 than 0.

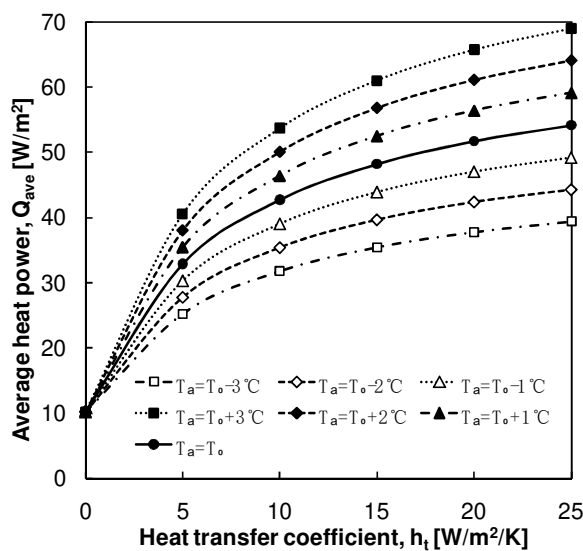


471
 472 (a) (b)
 473 **Fig. 8.** Variation of the instantaneous heat power per unit of tunnel lining surface ($T_a = T_0$) and the
 474 tunnel air temperature over 90 days for: (a) heating mode, and (b) cooling mode.

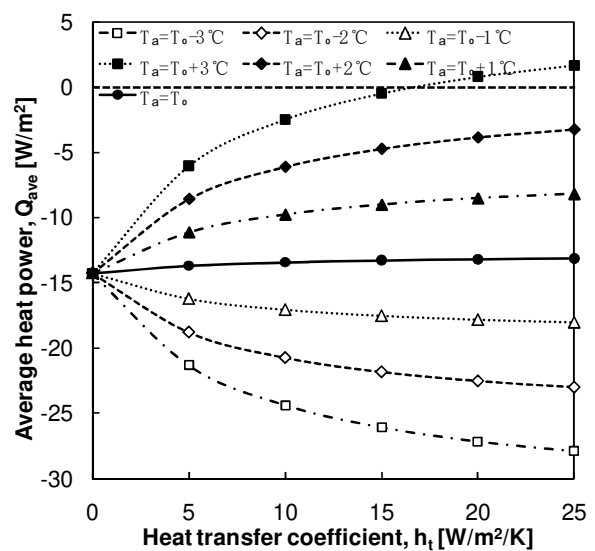
475 The average heat power increases by increasing the convective heat transfer coefficient
 476 h_t for all cases for the heating mode (Fig. 9a). However, its rise rate decreases for a
 477 successive increase of the heat transfer coefficient. For example, in the case where $T_a = T_0$ in
 478 heating mode, the average heat power increases by 10.6 W/m^2 , over an h_t range from
 479 $5 \text{ W/m}^2/\text{K}$ and $10 \text{ W/m}^2/\text{K}$, and only a $2.4 \text{ W/m}^2/\text{K}$ of difference is observed between the
 480 average heat power at $h_t = 20 \text{ W/m}^2/\text{K}$ and $25 \text{ W/m}^2/\text{K}$.

481 The same trend occurs when assessing the efficiency in the case where T_a is taken lower
 482 than T_0 for the cooling mode (Fig. 9b). However, the average injected heat power decreases
 483 as the heat transfer coefficient increases where T_a is equal to or greater than T_0 . This is

484 because the heat power improvement is also influenced by the temperature difference
485 between the tunnel air and the circulating fluid ($T_a - T_f$). For the heating mode (winter), since
486 all instantaneous tunnel air temperatures are always greater than the average circulating fluid
487 temperature (4.4 °C) during operation, the positive temperature difference allows the tunnel
488 environment to inject heat into the energy geostructure as a heat source. A higher heat transfer
489 coefficient then induces higher heat injection efficiency, and consequently, higher heat
490 extraction of circulating fluid can be achieved. For the cooling mode (summer), since the
491 average value of T_0 is closed to the temperature of circulating fluid (27.6 °C), the
492 instantaneous tunnel air temperature is generally lower than the circulating fluid temperature
493 when T_a is lower than T_0 . The negative temperature difference causes the tunnel environment
494 to extract heat from the energy tunnel lining (which is the goal of this functioning mode). In
495 such conditions, the injected heat power of the circulating fluid increases with increasing the
496 heat transfer coefficient. For $T_a \geq T_0$, the tunnel environment tends to inject heat to the energy
497 tunnel lining, and therefore the heat injection of the circulating fluid decreases with
498 increasing the heat transfer coefficient. In this sense, the efficiency of the system could be
499 compromised. Generally, a larger positive temperature difference for the heating mode or a
500 larger negative temperature difference for the cooling mode leads to a greater rise rate for
501 heat power extraction or injection with increasing the heat transfer coefficient.



(a)

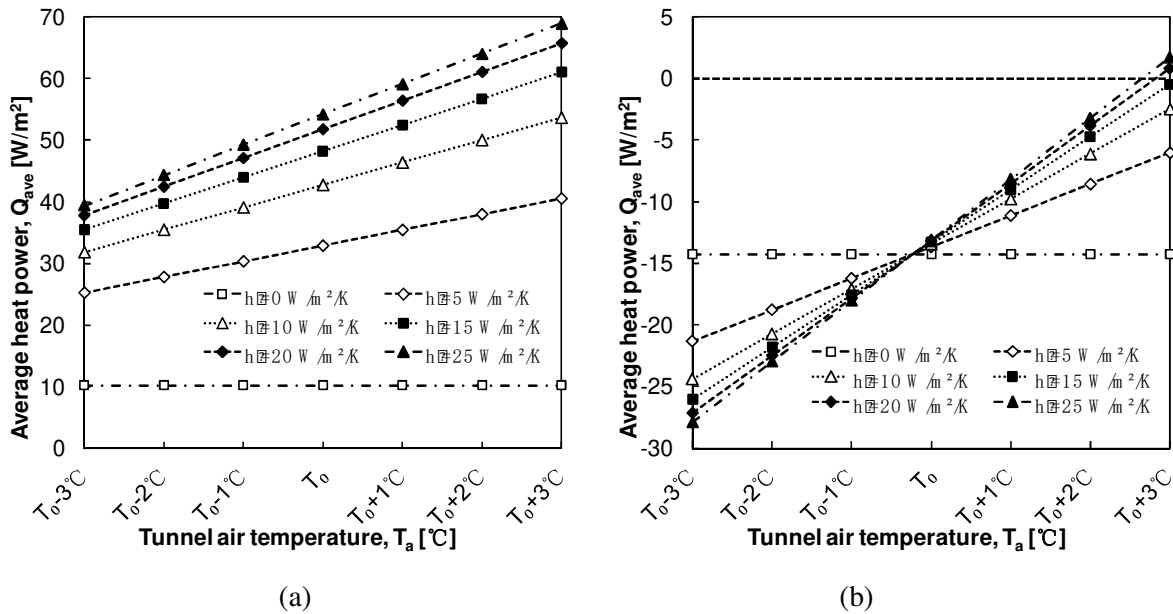


(b)

502
503

504 **Fig. 9.** Heat transfer coefficient effect on the average heat power due to differing tunnel air
 505 temperatures in: (a) heating mode, and (b) cooling mode, after 90-day activation.

506 Fig. 10a and Fig. 10b show a linear relationship between the average heat power and T_a .
 507 The average heat power during the study period differs for different T_a , but remains constant
 508 at 10.22 W/m^2 for the heating mode and -14.27 W/m^2 for the cooling mode when $h_t = 0$
 509 $\text{W/m}^2/\text{K}$. In these cases, the ground becomes the only energy resource to exchange heat with
 510 the circulating fluid as the air-lining boundary is considered as adiabatic. As a result, the
 511 value of average heat power reflects the ground heat exchange capacity. The heating mode
 512 results show that the heat exchanged by convection between the tunnel environment and the
 513 energy tunnel lining accounts for a large percentage of the total exchangeable heat. It is even
 514 greater than the ground extracted heat in all cases for the heating mode. Compared to the
 515 thermal insulation condition ($h_t=0 \text{ W/m}^2/\text{K}$), the thermal efficiency variation induced by the
 516 tunnel environment for the considered configurations in winter ranges between 147% to 574%
 517 and -112% to 95% in summer.

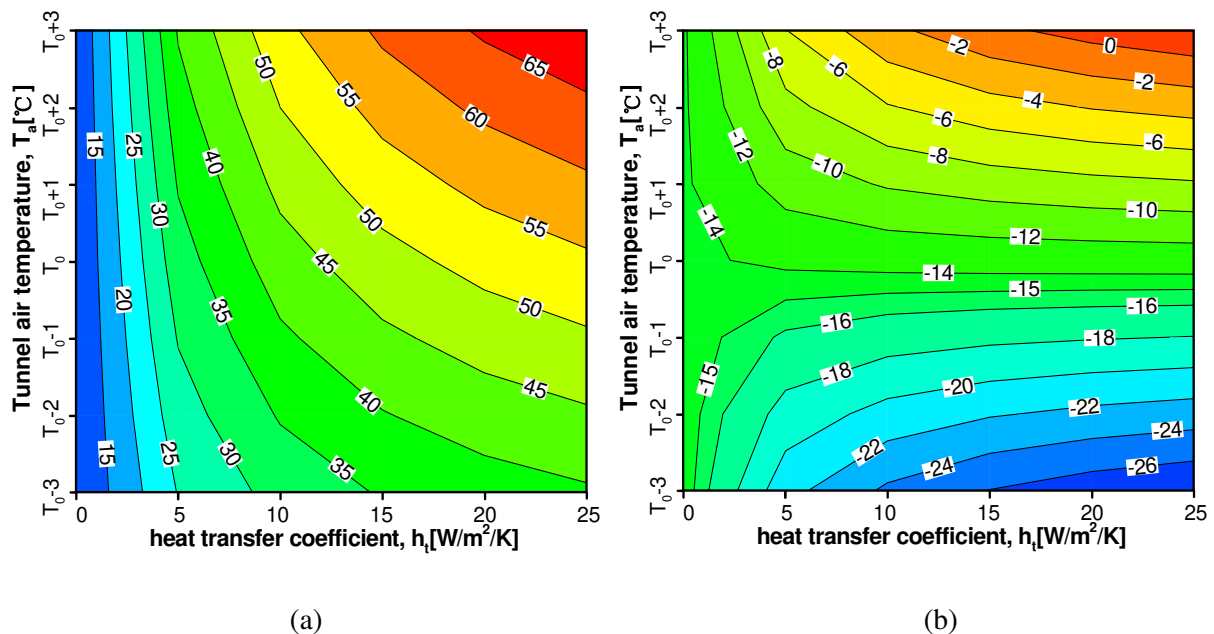


518
 519 (a) (b)
 520 **Fig. 10.** Tunnel air temperatures effect on the average heat power due to heat transfer coefficients in:
 521 (a) heating mode, and (b) cooling mode, after 90-day activation.

522 Design charts based on the results discussed above for heating mode (winter) and
 523 cooling (summer) were developed and can be seen in Fig. 11a and Fig. 11b respectively.

524 When varying the heat transfer coefficients and tunnel air temperatures, the heat exchange
 525 efficiency ranges in W/m^2 are indicated with different colours. Independently of the operation
 526 mode, the highest heat exchange rate is obtained for the maximum heat transfer coefficient,
 527 while the maximum positive temperature difference ($T_a - T_f$) leads to the maximum heat
 528 extraction rate in summer. The maximum positive temperature difference leads to the highest
 529 heat injection rate. As the heat transfer coefficient decreases, the tunnel air temperature effect
 530 becomes lower, since the contour lines slopes increase gradually. The average heat extraction
 531 rate involving the tunnel environment effect is usually in the range $10 - 65W/m^2$, and the heat
 532 injection rate varies between 0 and $-26W/m^2$. The heating mode chart is in good agreement
 533 with the recently one proposed by Dornberger et al. [42], but the cooling mode chart shows a
 534 different trend. This is due to the positive temperature difference between the tunnel air and
 535 the circulating fluid, which is different from literature one.

536 Based on the assumed conditions and geometry, the charts may provide optimistic
 537 results as do not take into account adjacent energy segmental linings. Thus, a more detailed
 538 study should be carried out at the design analysis stage. It is clear that these charts are
 539 typically applicable for cases with similar temperature difference among tunnel air,
 540 circulating fluid and ground. The ground water flow rate is not considered.



541
 542 (a) (b)
 543 **Fig. 11.** Design charts showing the average heat power in W/m^2 under different tunnel environment

544 conditions and for: (a) heating mode, and (b) cooling mode, after 90-day activation.

545 4.2. Tunnel environment influence on the heat power of system's components

546 The heat exchanged power in each zone can be expressed by its divergence intensity
547 induced by conduction and convection. Generally, the divergence of a zone as a heat source is
548 represented by a positive value, while a negative value for a zone represents a heat sink. In
549 this case, the geothermal system is comprised of three major components: the tunnel
550 environment, concrete lining and surrounding ground. The mechanism of heat exchange and
551 divergence in each zone can be obtained by the global method, which allows the calculation
552 of the instantaneous and average heat power in each component of the geothermal system
553 during the study period. It is important to note that no groundwater flow rate is considered in
554 this case study, therefore, the convective term divergence for the concrete lining and the
555 ground is null.

556 The conductive divergence distribution maps for two operation modes and two values of
557 the convective heat transfer coefficient after 90 days are plotted in Fig. 12 a,b,d and e ($T_a=T_0$).
558 It can be seen that the divergence is symmetrically distributed between the left and the right.
559 There is a slight difference between the top half and the bottom half section, because the
560 presence of water table (at 12m depth) makes the effective heat transfer coefficient and the
561 effective specific heat above the water surface lower than the ones below the water surface.
562 Considering the tunnel environment influence, even though the heat transfer coefficient is
563 small (e.g. $h_t = 5 \text{ W/m}^2/\text{K}$), the divergence variations of the lining and ground can be large,
564 thereby significantly affecting the heat power for each component. Fig. 12c and Fig. 12f
565 show that the tunnel environment and operating mode play a lower role in the divergence
566 disturbance range. For the heating mode, the conductive divergence in the lining and ground
567 varies between -0.5 W/m^3 and 0.65 W/m^3 (right vertical axis) with exception of the inner
568 tunnel lining wall (left vertical axis). As a heat source, the divergence intensity in the inner
569 lining wall is significantly higher than that in the other lining parts and the surrounding
570 ground. An exception appears when the air-lining boundary is considered as adiabatic (inner

571 lining divergence is equal to zero), and the divergence in the area around the absorber pipes
 572 shows negative peak values, as they act as a heat sink. When the circulating fluid is cooled,
 573 the opposite trend is expected to occur as shown in Fig. 12f. For both operation modes, the
 574 heat transfer coefficient variation results in the divergence change within the lining and
 575 ground. The position of the maximum divergence intensity in the ground occurs within 3.5 to
 576 4 meters from the air-lining interface, and moves slightly away from the tunnel hole when the
 577 heat transfer coefficient increases.

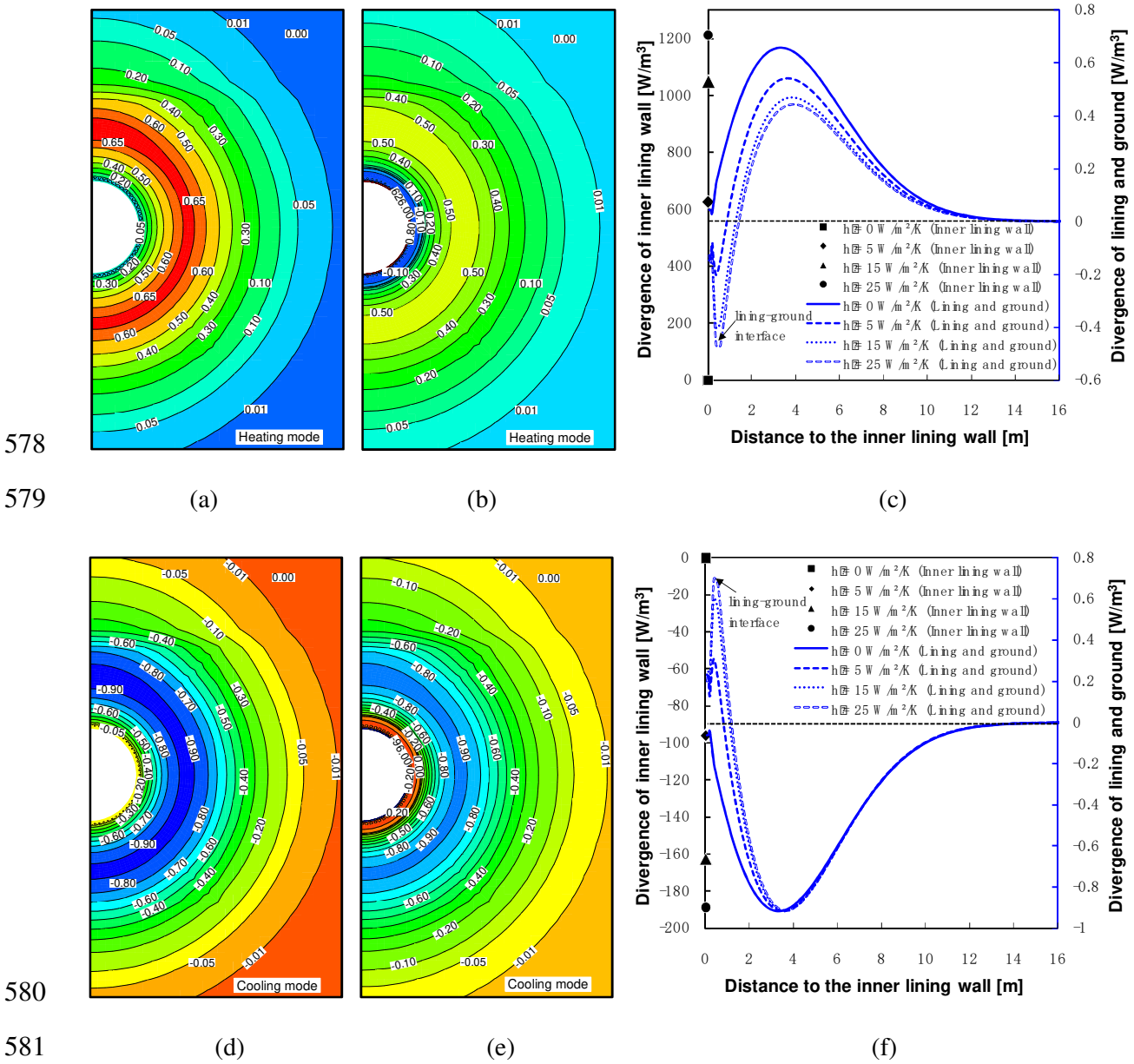
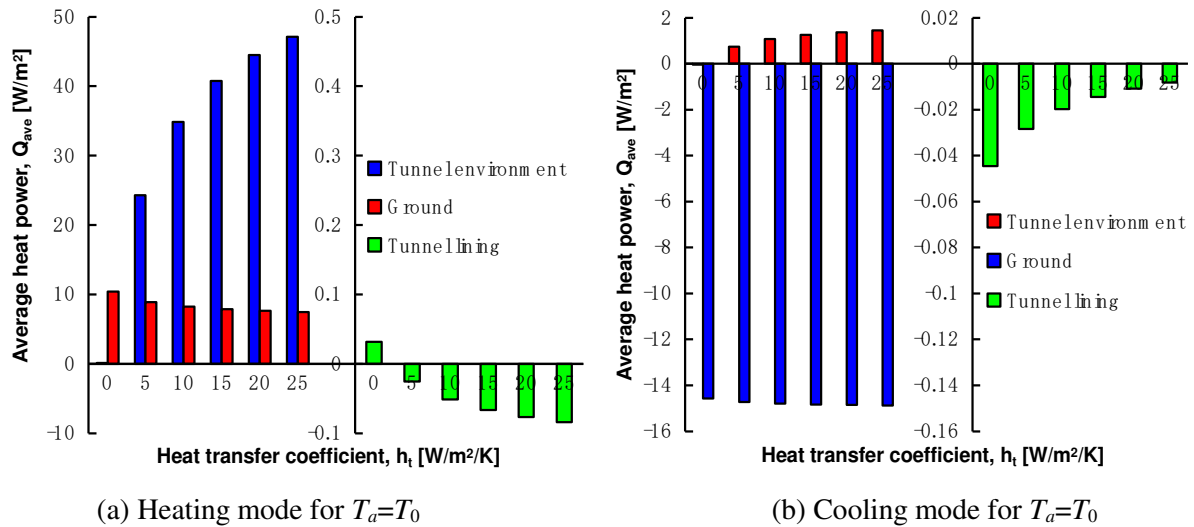


Fig. 12. Conductive divergence variations around the tunnel: (a) heating mode for $h_t = 0 \text{ W/m}^2/\text{K}$, (b) heating mode for $h_t = 5 \text{ W/m}^2/\text{K}$, (c) variations along horizontal direction for heating mode, (d) cooling mode for $h_t = 0 \text{ W/m}^2/\text{K}$, (e) cooling mode for $h_t = 5 \text{ W/m}^2/\text{K}$, (f) variations along horizontal direction for cooling mode.

584 cooling mode for $h_t = 0$ W/m²/K, (e) cooling mode for $h_t = 5$ W/m²/K, (f) variations along horizontal
585 direction for cooling mode.

586 After obtaining the divergence of each zone, one can thus derive the average heat power
587 per tunnel lining surface unit provided by each system's component (Fig. 13). The term
588 "tunnel environment" refers to the average heat power obtained from the inner tunnel lining
589 wall, while the other lining parts are represented by the term "tunnel lining". The heat
590 exchanged with the tunnel lining is almost negligible compared with the heat transferred by
591 thermal conduction through the other two components. For the heating mode, the nonzero
592 heat transfer coefficient induces that the tunnel lining extract heat from the ambient
593 environment, resulting in its temperature rise and thus the negative average heat
594 power/divergence (Fig. 13a).

595 It can be seen from Fig. 12c and Fig. 13a that although the heat transfer coefficient
596 increase leads to a lower divergence value for the heating mode, which results in a reduction
597 in the instantaneous heat power gained from the ground, greater total heat power can be
598 obtained due to the significant increase in divergence density in the inner lining wall [12].
599 The tunnel environment is the primary source of heat extraction in winter, whereas the
600 ground constitutes the main part for the heat injection in summer (Fig. 13b). The reason for
601 this phenomenon is attributed to the temperature difference as the key factor discussed
602 previously. Additionally, the positive average temperature difference in cooling mode during
603 the study period does not favor heat injection to the tunnel environment, thus reducing the
604 total system efficiency.



605

606

607

Fig. 13. Average heat power in each system's component against the heat transfer coefficient.

608

609

610

611

612

613

614

615

616

617

618

619

620

621

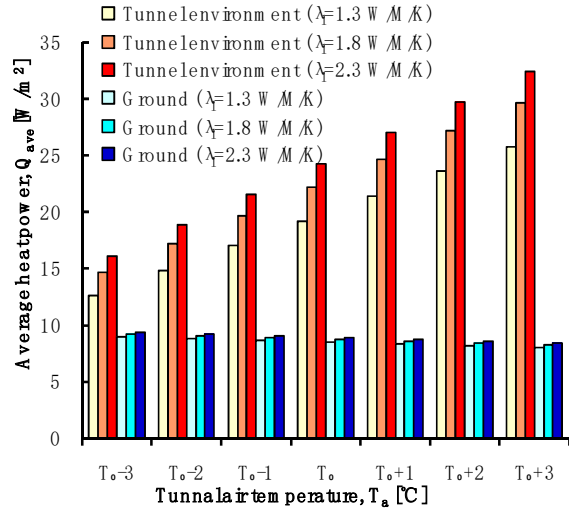
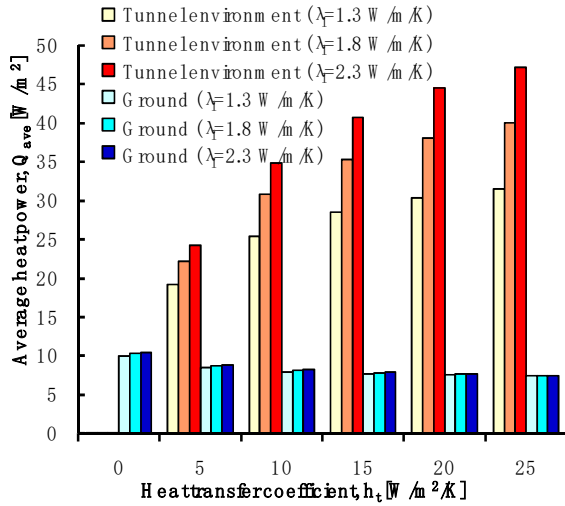
622

623

624

625

Since the lining is the medium between the tunnel environment and the absorber pipes, the contribution of the tunnel environment is expected to be highly influenced by the concrete lining thermal properties as well. In order to understand the role of tunnel lining thermal properties in the energy performance, the effect of thermal conductivity of the reinforced concrete was studied through a parametric analysis, by varying it in a reasonable range according to [43]. Only the different heating mode configurations were investigated because the tunnel environment influence on the heat power variation is more pronounced compared to the cooling mode influence. As shown in Fig. 14, the heat power variation in each component shows the same trend as Fig. 13, i.e. the non-linear increase with the heat transfer coefficient and the linear increase with the temperature difference between the tunnel air and the circulating fluid. However, the increase or decrease rate of average heat power in each component is affected by the thermal conductivity variation. Increasing the tunnel lining thermal conductivity can facilitate the tunnel environment effect on the energy performance. Increasing the thermal conductivity for the heating mode can cause an increase of the total average heat power by around 40% and 21% when considering respectively the maximum heat transfer coefficient ($T_a=T_0$) and the maximum tunnel air temperature ($h_t=5 W/m^2/K$). These results show that a special attention needs to be given to the tunnel lining thermal properties when assessing the tunnel environment impact.



626

627

(a) Heating mode for $T_a=T_0$

(b) Heating mode for $h_t=5$ W/m²/K

628

Fig. 14. Average heat power in each system's component at indicated thermal conductivity of lining

629

against: (a) heat transfer coefficient and (b) tunnel air temperature.

630

5. Conclusion

631

This work presents a numerical analysis of the thermal performance of energy tunnel

632

linings based on the geometry and geological conditions of the Torino Metro Line 1 section.

633

It allows to better understand how the heat transfer behaviour of an energy tunnel is affected

634

by the tunnel environment. Two numerical approaches were introduced and validated to

635

calculate the heat exchange efficiency of the model. The main conclusions are as follows:

636

- The tunnel environment has a crucial role in the thermal performance of an energy

637

tunnel. The average heat power variation depends on the temperature difference between the

638

tunnel air and the circulating fluid. The larger the heat transfer coefficient, the greater

639

magnitude of the heat exchange,

640

- The heat exchange efficiency shows a non-linear relationship with the heat transfer

641

coefficient and a linear relationship with the temperature difference between the tunnel air

642

and the circulating fluid. The presented design charts for different tunnel environments can be

643

used for the first assessment of a site where similar temperature differences and underground

644

conditions can be found,

645

- The change of tunnel environment affects not only the heat exchange between tunnel

646 air and geothermal system, but also the amount of energy exchanged with the ground,
647 however, it has little impact on the volume affected by the heat exchange in the ground. The
648 ground area with the maximum heat exchange rate is usually located between 3.5 to 4 m from
649 the air-lining boundary after a 90-day operation,

650 • In winter, the heat exchange is primarily done with the tunnel environment. In summer,
651 most of the heat is injected into the ground,

652 • For the heating mode, maximum improvement of 40% and 21% can be achieved by
653 varying the thermal conductivity of tunnel lining for various heat transfer coefficients and
654 tunnel air temperatures. Therefore, to guarantee a reasonable estimation of the tunnel
655 environment effect on energy performance, special attention should also be paid to the
656 concrete lining thermal properties.

657 It is important to note that some results in this study cannot be considered as general to
658 evaluate the energy exploitation potential of an energy tunnel. A more detailed study should
659 be carried out at the design stage, which should include detailed aspects of the specific site
660 installation and working conditions.

661 **Data availability statements**

662 Some or all data, models, or code that support the findings of this study are available
663 from the corresponding author upon reasonable request.

664 **Acknowledgements**

665 The authors gratefully acknowledge the financial support provided by the China
666 Scholarship Council (201809210024). The laboratory 3SR is part of the LabEx Tec 21
667 (Investissement d'avenir - grant agreement n. ANR-11-LABX-0030).

668 **References**

- 669 [1] GLOBALABC, Global Alliance for Buildings and Construction, 2018 Global Status Report, (2018) 12.
670 [2] F. Loveridge, J.S. McCartney, G.A. Narsilio, M. Sánchez, Energy geostructures: a review of analysis
671 approaches, in situ testing and model scale experiments., Geomech. Energy Environ. (2019) in press.

- 672 <https://doi.org/10.1016/j.gete.2019.100173>.
- 673 [3] J.C. Choi, S.R. Lee, D.S. Lee, Numerical simulation of vertical ground heat exchangers: Intermittent
674 operation in unsaturated soil conditions, *Comput. Geotech.* 38 (2011) 949–958.
675 <https://doi.org/10.1016/j.compgeo.2011.07.004>.
- 676 [4] L. Laloui, A. Di Donna, *Energy Geostrutures: Innovation in Underground Engineering*, 2013.
677 <https://doi.org/10.1002/9781118761809>.
- 678 [5] M. Barla, A. Di Donna, Energy tunnels: concept and design aspects, *Undergr. Sp.* 3 (2018) 268–276.
679 <https://doi.org/10.1016/j.undsp.2018.03.003>.
- 680 [6] K. Soga, Y. Rui, Energy geostrutures, in: *Adv. Ground-Source Heat Pump Syst.*, 2016.
681 <https://doi.org/10.1016/B978-0-08-100311-4.00007-8>.
- 682 [7] H. Brandl, Energy foundations and other thermo-active ground structures, *Geotechnique.* 56 (2006) 81–
683 122. <https://doi.org/10.1680/geot.2006.56.2.81>.
- 684 [8] B. Cousin, A.F. Rotta Loria, A. Bourget, F. Rognon, L. Laloui, Energy performance and economic
685 feasibility of energy segmental linings for subway tunnels, *Tunn. Undergr. Sp. Technol.* 91 (2019)
686 102997. <https://doi.org/10.1016/j.tust.2019.102997>.
- 687 [9] A. Revesz, I. Chaer, J. Thompson, M. Mavroulidou, M. Gunn, G. Maidment, Ground source heat pumps
688 and their interactions with underground railway tunnels in an urban environment: A review, *Appl.*
689 *Therm. Eng.* 93 (2016) 147–154. <https://doi.org/10.1016/j.applthermaleng.2015.09.011>.
- 690 [10] J. Wilhelm, L. Rybach, The geothermal potential of Swiss Alpine tunnels, *Geothermics.* 32 (2003) 557–
691 568. [https://doi.org/10.1016/S0375-6505\(03\)00061-0](https://doi.org/10.1016/S0375-6505(03)00061-0).
- 692 [11] S. Frodl, J.N. Franzius, T. Bar, Planung und bau der tunnel-geothermieanlage in Jenbach, *Geomech.*
693 *Und Tunnelbau.* 3 (2010) 658–668. <https://doi.org/10.1002/geot.201000037>.
- 694 [12] M. Barla, A. Di Donna, M. Baralis, City scale analysis of subsoil thermal conditions due to geothermal
695 exploitation, *Environ. Geotech.* (2018) 1–41. <https://doi.org/10.1680/jenge.17.00087>.
- 696 [13] M. Baralis, M. Barla, W. Bogusz, A. Di Donna, G. Ryżyński, M. Żeruń, Geothermal potential of the NE
697 extension Warsaw (Poland) metro tunnels, *Environ. Geotech.* (2018) 1–13.
698 <https://doi.org/10.1680/jenge.18.00042>.
- 699 [14] M. Barla, A. Di Donna, A. Insana, A novel real-scale experimental prototype of energy tunnel, *Tunn.*

- 700 Undergr. Sp. Technol. 87 (2019) 1–14. <https://doi.org/10.1016/j.tust.2019.01.024>.
- 701 [15] J.N. Franzius, N. Pralle, Turning segmental tunnels into sources of renewable energy, Proc. Inst. Civ.
702 Eng. Civ. Eng. 164 (2011) 35–40. <https://doi.org/10.1680/cien.2011.164.1.35>.
- 703 [16] M. Barla, A. Di Donna, Conci energetici per il rivestimento delle gallerie, Strade & Autostrade. 5 (2016)
704 2–5.
- 705 [17] D.P. Nicholson, Q. Chen, A. Pillai, M. Chendorain, Developments in thermal piles and thermal tunnel
706 lining for city scale GSHP systems, Thirty-Eighth Work. Geotherm. Reserv. Eng. (2013) 1437–1444.
- 707 [18] G. Zhang, S. Liu, X. Zhao, M. Ye, R. Chen, H. Zhang, J. Yang, J. Chen, The coupling effect of
708 ventilation and groundwater flow on the thermal performance of tunnel lining GHEs, Appl. Therm. Eng.
709 (2017). <https://doi.org/10.1016/j.applthermaleng.2016.10.120>.
- 710 [19] A. Bidarmaghz, G.A. Narsilio, Heat exchange mechanisms in energy tunnel systems, Geomech. Energy
711 Environ. 16 (2018) 83–95. <https://doi.org/10.1016/j.gete.2018.07.004>.
- 712 [20] F. Tinti, D. Boldini, M. Ferrari, M. Lanconelli, S. Kasmaee, R. Bruno, H. Egger, A. Voza, R. Zurlo,
713 Exploitation of geothermal energy using tunnel lining technology in a mountain environment. A
714 feasibility study for the Brenner Base tunnel – BBT, Tunn. Undergr. Sp. Technol. 70 (2017) 182–203.
715 <https://doi.org/10.1016/j.tust.2017.07.011>.
- 716 [21] P.J. Bourne-Webb, T.M. Bodas Freitas, R.A. Da Costa Gonçalves, Thermal and mechanical aspects of
717 the response of embedded retaining walls used as shallow geothermal heat exchangers, Energy Build.
718 125 (2016) 130–141. <https://doi.org/10.1016/j.enbuild.2016.04.075>.
- 719 [22] M. Peltier, A.F. Rotta Loria, L. Lepage, E. Garin, L. Laloui, Numerical investigation of the convection
720 heat transfer driven by airflows in underground tunnels, Appl. Therm. Eng. 159 (2019) 113844.
721 <https://doi.org/10.1016/j.applthermaleng.2019.113844>.
- 722 [23] A. Insana, M. Barla, Experimental and numerical investigations on the energy performance of a
723 thermo-active tunnel, Renew. Energy. 152 (2020) 781–792.
724 <https://doi.org/10.1016/j.renene.2020.01.086>.
- 725 [24] S.W. Rees, M.H. Adjali, Z. Zhou, M. Davies, H.R. Thomas, Ground heat transfer effects on the thermal
726 performance of earth-contact structures, Renew. Sustain. Energy Rev. 4 (2000) 213–265.
727 [https://doi.org/10.1016/S1364-0321\(99\)00018-0](https://doi.org/10.1016/S1364-0321(99)00018-0).

- 728 [25] O.T. Farouki, Thermal properties of soils, Cold regions research and engineering lab hanover, NH,
729 1981.
- 730 [26] O. Ogunleye, R.M. Singh, F. Cecinato, J. Chan Choi, Effect of intermittent operation on the thermal
731 efficiency of energy tunnels under varying tunnel air temperature, *Renew. Energy*. 146 (2020) 2646–
732 2658. <https://doi.org/10.1016/j.renene.2019.08.088>.
- 733 [27] F. Cecinato, F.A. Loveridge, Influences on the thermal efficiency of energy piles, *Energy*. 82 (2015)
734 1021–1033. <https://doi.org/10.1016/j.energy.2015.02.001>.
- 735 [28] M. Barla, A. Di Donna, A. Perino, Application of energy tunnels to an urban environment, *Geothermics*.
736 61 (2016) 104–113. <https://doi.org/10.1016/j.geothermics.2016.01.014>.
- 737 [29] A. Di Donna, F. Cecinato, F. Loveridge, M. Barla, Energy performance of diaphragm walls used as heat
738 exchangers, *Proc. Inst. Civ. Eng. Geotech. Eng.* 170 (2017) 232–245.
739 <https://doi.org/10.1680/jgeen.16.00092>.
- 740 [30] F. W. Dittus and L. M. K. Boelter, Heat transfer in automobile radiators of the tubular type, University
741 of California Publications of Engineering, 1930.
- 742 [31] C.C. Wang, C.B. Chiou, D.C. Lu, Single-phase heat transfer and flow friction correlations for microfin
743 tubes, *Int. J. Heat Fluid Flow*. 17 (1996) 500–508. [https://doi.org/10.1016/0142-727X\(96\)00048-3](https://doi.org/10.1016/0142-727X(96)00048-3).
- 744 [32] V. Gnielinski, New equations for heat and mass transfer in turbulent pipe and channel flow, *Int. Chem.*
745 *Eng.* 16 (1976) 359–368.
- 746 [33] M. Hallquits, Heat Transfer and Pressure Drop Characteristics of Smooth Tubes At a Constant Heat
747 Flux in the Transitional Flow Regime, (2011) 1–145.
- 748 [34] D.P. Nicholson, Q. Chen, M. De Silva, A. Winter, R. Winterling, The design of thermal tunnel energy
749 segments for Crossrail, UK, *Proc. Inst. Civ. Eng. Eng. Sustain.* 167 (2014) 118–134.
750 <https://doi.org/10.1680/ensu.13.00014>.
- 751 [35] R.A. Beier, Vertical temperature profile in ground heat exchanger during in-situ test, *Renew. Energy*. 36
752 (2011) 1578–1587. <https://doi.org/10.1016/j.renene.2010.10.025>.
- 753 [36] L. Zhang, Q. Zhang, G. Huang, Y. Du, A p(t)-linear average method to estimate the thermal parameters
754 of the borehole heat exchangers for in situ thermal response test, *Appl. Energy*. 131 (2014) 211–221.
755 <https://doi.org/10.1016/j.apenergy.2014.06.031>.

- 756 [37] A. Di Donna, M. Barla, The role of ground conditions on energy tunnels' heat exchange, *Environ.*
757 *Geotech.* 3 (2016) 214–224. <https://doi.org/10.1680/jenge.15.00030>.
- 758 [38] D. Rammal, Thermo-mechanical behaviour of geothermal structures: numerical modelling and
759 recommendations, Université Lille 1, 2017.
- 760 [39] Y. Delerablee, S. Burlon, P. Reiffsteck, Long-term assessment of thermal sustainability of thermoactive
761 geostructures, *Environ. Geotech.* (2019) 1–17. <https://doi.org/10.1680/jenge.17.00102>.
- 762 [40] G. Zhang, C. Xia, M. Sun, Y. Zou, S. Xiao, A new model and analytical solution for the heat conduction
763 of tunnel lining ground heat exchangers, *Cold Reg. Sci. Technol.* 88 (2013) 59–66.
764 <https://doi.org/10.1016/j.coldregions.2013.01.003>.
- 765 [41] C. Lee, S. Park, J. Won, J. Jeoung, B. Sohn, H. Choi, Evaluation of thermal performance of energy
766 textile installed in Tunnel, *Renew. Energy.* 42 (2012) 11–22.
767 <https://doi.org/10.1016/j.renene.2011.09.031>.
- 768 [42] S.C. Dornberger, A.F. Rotta Loria, M. Zhang, L. Bu, J.L. Epard, P. Turberg, Heat exchange potential of
769 energy tunnels for different internal airflow characteristics, *Geomech. Energy Environ.* (2020) 100229.
770 <https://doi.org/10.1016/j.gete.2020.100229>.
- 771 [43] S. Zhao, S. Yang, X. Feng, M. Lu, Study on Thermal Conductivity of Reinforced Concrete Plate Study
772 on Thermal Conductivity of Reinforced Concrete Plate, (2016).
773 <https://doi.org/10.4028/www.scientific.net/AMM.438-439.321>.
- 774